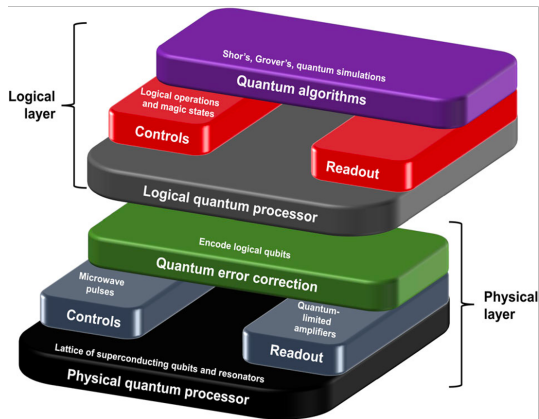


Contents

- 1 Overview
- 2 Physical Process
- 3 Calibration of Experimental Parameters
- 4 Summary

Quantum Computing Architecture

How to build a Quantum Computer?



- **Superconducting** quantum computing
- **Photonic** quantum computing
- **quantum dots** quantum computing
- **Trapped-ion** quantum computing

Comparing the Characteristics of different types of QC¹

Superconducting QC

Pros

- Fast working
- Build on existing semiconductor industry

Cons

- Collapse easily and must be kept in cold

Photonics QC

Pros

- CMOS compatible photonics waveguide technology

Cons

- Cryogenic single photon sources and detectors

Trapped-Ion QC

Pros

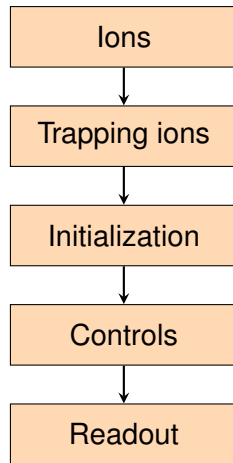
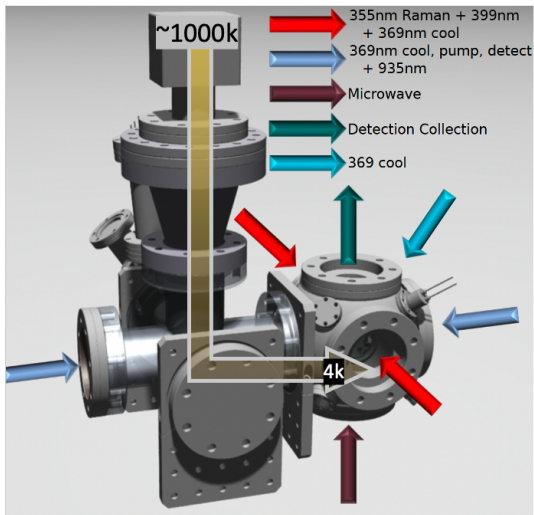
- Very stable > 1000s
- Highest achieved gate fidelities (e.g. two-qubit gate 99.9%)
- Fully connected

Cons

- Scalability
- Slow operation

¹Bruzewicz et al. 2019

Quantum Computing with Trapped Ions



Vibration Modes

Canonical Hamiltonian

$$\hat{H} = \sum_{j=1}^N \left(\frac{1}{2m} \hat{p}_j^2 + \frac{m}{2} \omega_m^2 \hat{q}_j^2 \right)$$

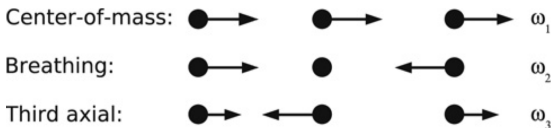
Quantization

$$\hat{q} = \sqrt{\frac{\hbar}{2m\omega}} (\hat{a} + \hat{a}^\dagger)$$

$$\hat{p} = -i\sqrt{\frac{\hbar m\omega}{2}} (\hat{a} - \hat{a}^\dagger)$$

Kinetic term

$$\hat{H}_m = \hbar\omega \left(\hat{a}^\dagger \hat{a} + \frac{1}{2} \right) \sim \hbar\omega \hat{a}^\dagger \hat{a}$$



When N oscillators are coupled, N different canonical modes are obtained, which correspond to **phonons of N different frequencies**.

Two-level Approximation and Raman Process

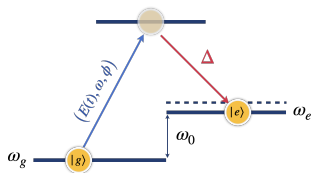


Figure: Internal energy level transition of ions

- Two-level approximation for electronic energy levels

$$\hat{H}_e = \hbar (\omega_g |g\rangle \langle g| + \omega_e |e\rangle \langle e|) \sim \hbar \frac{\omega_0}{2} \hat{\sigma}_z$$

- Interaction term

$$\hat{H}_{int} = \frac{\hbar}{2} \Omega (|e\rangle \langle g| + |g\rangle \langle e|) \left[e^{i(kx - \omega t + \phi)} + e^{-i(kx - \omega t + \phi)} \right]$$

Why is it necessary to go through a ‘bridge’?

- 1 It is difficult to produce a laser at the GHz level.
- 2 There may be an electric dipole forbidden transition between the $|g\rangle$ and $|e\rangle$ states.
- 3 Many factors, like laser intensity, phase, and frequency, can affect the direct transition from $|g\rangle$ to $|e\rangle$, leading to operational inaccuracies.

The Basic Hamiltonian

1 Trans to interaction picture

$$H'_{int} = e^{iH_0 t/\hbar} H_{int} e^{-iH_0 t/\hbar}$$

2 $kx = kx_0 (\hat{a} + \hat{a}^\dagger) = \eta (\hat{a} + \hat{a}^\dagger)$

3 Rotating wave approximation

4 Lamb-Dicke approximations $\eta \sqrt{\langle (\hat{a}^\dagger + \hat{a})^2 \rangle} \ll 1$

Lamb-Dicke Parameter η

$$\eta = k_x x_0 = k_x \sqrt{\langle 0 | x^2 | 0 \rangle} = k_x \sqrt{\frac{\hbar}{2m\omega_x}}$$

η quantifies the coupling strength between the internal and motional states of the ion.

The Basic Hamiltonian

$$H \approx \frac{\hbar}{2} \hat{\sigma}_+ \left[1 + i\eta \left(\hat{a}^\dagger e^{i\omega_m t} + \hat{a} e^{-i\omega_m t} \right) \right] e^{i(\phi - \mu t)} + \text{h.c.}$$

- Carrier transition $|g\rangle |n\rangle \leftrightarrow |e\rangle |n\rangle$ ($\mu = 0$)

$$H_{\text{car}} = \frac{\hbar}{2} \Omega \left(\hat{\sigma}_+ e^{i\phi} + \hat{\sigma}_- e^{-i\phi} \right)$$

- Blue sideband transition $|g\rangle |n\rangle \leftrightarrow |e\rangle |n+1\rangle$ ($\mu = \omega_m + \delta$)

$$H_{\text{bsb}} = i\eta \frac{\hbar}{2} \Omega \left(\hat{\sigma}_+ \hat{a}^\dagger e^{i\phi} e^{-i\delta t} + \hat{\sigma}_- \hat{a} e^{-i\phi} e^{i\delta t} \right)$$

- Red sideband transition $|g\rangle |n\rangle \leftrightarrow |e\rangle |n-1\rangle$ ($\mu = -\omega_m - \delta$)

$$H_{\text{rsb}} = i\eta \frac{\hbar}{2} \Omega \left(\hat{\sigma}_+ \hat{a} e^{i\phi} e^{i\delta t} - \hat{\sigma}_- \hat{a}^\dagger e^{-i\phi} e^{-i\delta t} \right)$$

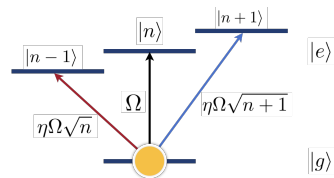


Figure: Transitions

Single-Qubit Gates

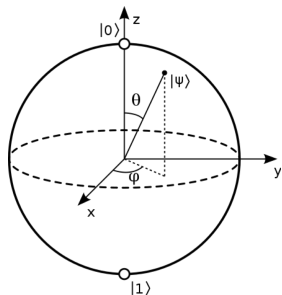


Figure: Bloch sphere

Carrier transition

$$H_{\text{car}} = \frac{\hbar}{2} \Omega \left(\hat{\sigma}_+ e^{i\varphi} + \hat{\sigma}_- e^{-i\varphi} \right)$$

The system can realize a rotation of angle $\theta/2 = \Omega t/2$ around any axis (φ) in the x-y plane under the action of H_{car} after free evolution for a time t .

$$R(\theta, \varphi) = e^{-iH_{\text{car}}t/\hbar} = \begin{pmatrix} \cos \frac{\theta}{2} & ie^{i\varphi} \sin \frac{\theta}{2} \\ ie^{-i\varphi} \sin \frac{\theta}{2} & \cos \frac{\theta}{2} \end{pmatrix}$$

- $R_x(\theta) = R(\theta, \varphi = 0) = \begin{pmatrix} \cos \frac{\theta}{2} & -i \sin \frac{\theta}{2} \\ -i \sin \frac{\theta}{2} & \cos \frac{\theta}{2} \end{pmatrix}$
- $R_y(\theta) = R(\theta, \varphi = \pi/2) = \begin{pmatrix} \cos \frac{\theta}{2} & -\sin \frac{\theta}{2} \\ \sin \frac{\theta}{2} & \cos \frac{\theta}{2} \end{pmatrix}$

Two-Qubit Gates

Cirac-Zoller Gate²

Red sideband transition

$$H_{\text{rsb}} = i\eta\frac{\hbar}{2}\Omega \left(\hat{\sigma}_+ \hat{a} e^{i\phi} e^{i\delta t} - \hat{\sigma}_- \hat{a}^\dagger e^{-i\phi} e^{-i\delta t} \right)$$

	(1)	(2)	(3)
① Apply a π -pulse on ion A	$ gg0\rangle \rightarrow$	$ gg0\rangle \rightarrow$	$ gg0\rangle \rightarrow$
② Apply a 2π -pulse on ion B	$ ge0\rangle \rightarrow$	$ ge0\rangle \rightarrow$	$ ge0\rangle \rightarrow$
③ Apply a π -pulse on ion A again	$ eg0\rangle \rightarrow -i gg1\rangle$	$ eg0\rangle \rightarrow i gg1\rangle$	$ eg0\rangle \rightarrow$
	$ ee0\rangle \rightarrow -i ge1\rangle$	$ ee0\rangle \rightarrow -i ge1\rangle$	$ ee0\rangle \rightarrow - ee0\rangle$

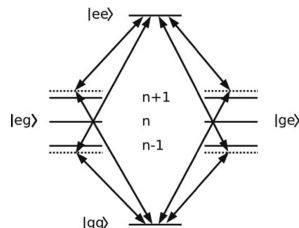
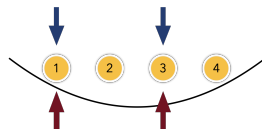
$$|\pm\rangle = (|g\rangle \pm |e\rangle)/\sqrt{2} \quad \Rightarrow \quad \begin{array}{l} |g\rangle |\pm\rangle \rightarrow |g\rangle |\pm\rangle \\ |e\rangle |\pm\rangle \rightarrow |e\rangle |\mp\rangle \end{array} \quad \Rightarrow \quad \text{Controlled-Z Gate!}$$

²Cirac and Zoller 1995

Two-Qubit Gates

Mølmer-Sørensen Gate

By simultaneously applying a two-frequency laser beam $\omega_0 \pm (\omega_m + \delta)$ to two ions separately, it is possible to drive the red sideband transition and the blue sideband transition of the ions at the same time.



- Red sideband transition

$$H_{rsb} = i\eta \frac{\hbar}{2} \Omega \left(\hat{\sigma}_+ \hat{a} e^{i\phi} e^{i\delta t} - \hat{\sigma}_- \hat{a}^\dagger e^{-i\phi} e^{-i\delta t} \right)$$

- Blue sideband transition

$$H_{bsb} = i\eta \frac{\hbar}{2} \Omega \left(\hat{\sigma}_+ \hat{a}^\dagger e^{i\phi} e^{-i\delta t} + \hat{\sigma}_- \hat{a} e^{-i\phi} e^{i\delta t} \right)$$

$$H_{MS} = \sum_{j=1}^2 (H_{rsb} + H_{bsb})$$

Two-Qubit Gates

Mølmer-Sørensen Gate

$$U(t_g) = \exp \left[-i \sum_j^M \hat{\sigma}_x^j \sum_{k=1}^N \left(\alpha_{j,k}(t_g) \hat{a}_k^\dagger - \alpha_{j,k}^*(t_g) \hat{a}_k \right) + i \sum_{m < n}^M \chi_{m,n}(t_g) \hat{\sigma}_x^m \hat{\sigma}_x^n \right]$$

where

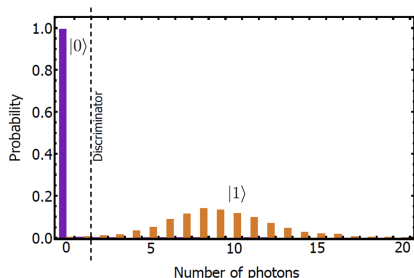
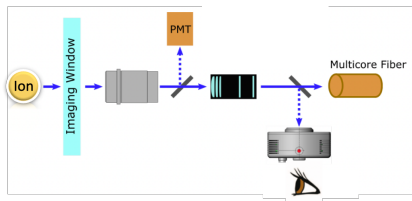
$$\alpha_{j,k}(t_g) = \int_0^{t_g} dt f(\eta_{k,j}, \Omega_j(t), \omega_k), \quad \chi_{m,n}(t_g) = \sum_k \int_0^{t_g} dt \int_0^t dt_1 g(\eta_{k,j}, \Omega_m(t), \Omega_n(t_1), \omega_k)$$

When $\alpha_{j,k}(t_g) \rightarrow 0$ and $\chi_{m,n}(t_g) \rightarrow \pi/4$, the **maximum entangled state** is obtained:

$$\begin{aligned} |gg\rangle &\rightarrow (|gg\rangle + i|ee\rangle)/\sqrt{2} \\ |ee\rangle &\rightarrow (|ee\rangle + i|gg\rangle)/\sqrt{2} \\ |ge\rangle &\rightarrow (|ge\rangle - i|eg\rangle)/\sqrt{2} \\ |eg\rangle &\rightarrow (|eg\rangle - i|ge\rangle)/\sqrt{2} \end{aligned}$$

Readout

Resonance Fluorescence Method



- Fluorescence detected: $|1\rangle$
- Fluorescence NOT detected: $|0\rangle$

- Measurement readout fidelity $> 99.999\%$
- Single measurement time $\sim 150\mu\text{s}$

Calibration

Motivation

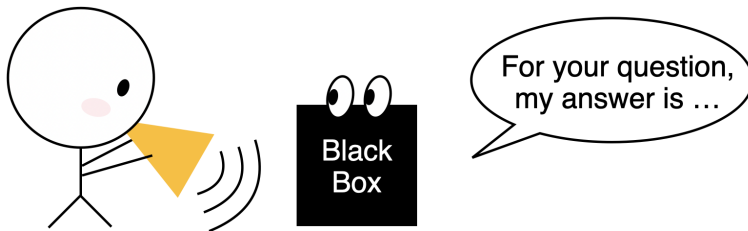
Factors limiting the fidelity (physical layer)

- 1 Decoherence
- 2 Preparation error
- 3 **Imprecise of experimental parameters**
(e.g. phonon frequency ω_k , Lamb-Dicke parameter η , \dots)

General Calibration Schemes for Ion Trap Systems

- 1 Insufficient automation
- 2 Low efficiency
- 3 Poor accuracy

Calibration



$$H = \sum_{j,k} H_{j,k} = \hbar \sum_j \frac{\Omega_j}{2} \hat{\sigma}_j^+ e^{i(\phi_j - \mu_j t)} \sum_k \exp \left[i \eta_{j,k} \left(\hat{a}_k^\dagger e^{i\omega_k t} + \hat{a}_k e^{-i\omega_k t} \right) \right] + \text{h.c.}$$

- 1 Calibrating the phonon frequencies ω_k
- 2 Calibrating the Lamb-Dicke parameters $\eta_{j,k}$

Calibration of Phonon Frequency

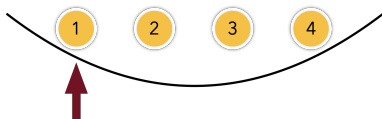
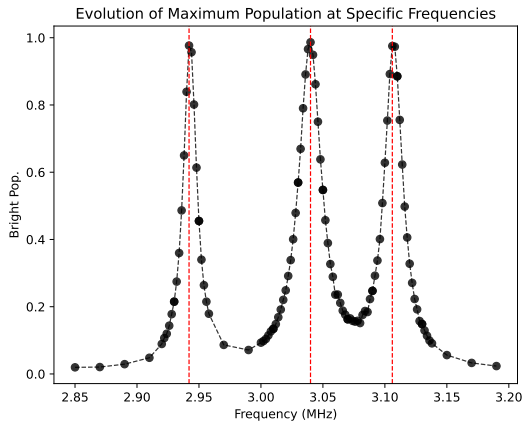
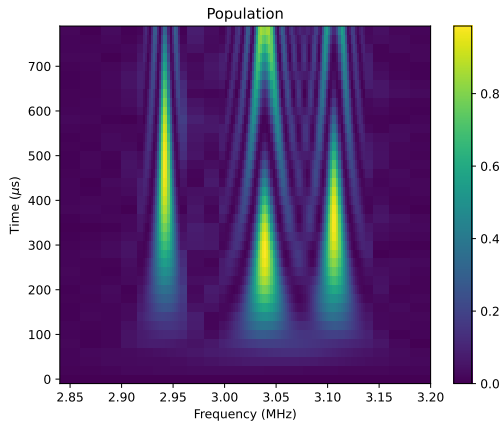


Figure: Calibration of phonon frequencies

Changing the laser frequency and recording the evolution of the ions at different frequencies.

Calibration of Phonon Frequency



Calibration of Phonon Frequency

Example: 3 ions with 3 phonons.

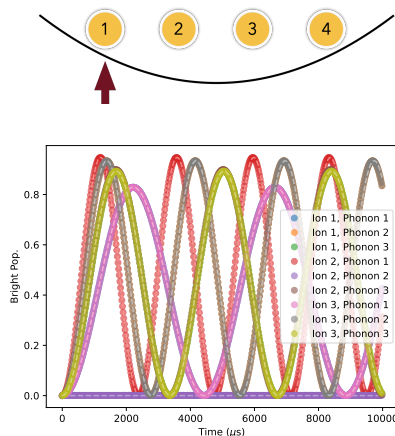
	Phonon frequency	Calibrated Phonon frequency	Error
ω_1	2.9574 MHz	2.9574 MHz	−0.0154 MHz
ω_2	3.0542 MHz	3.040 MHz	−0.0142 MHz
ω_3	3.1222 MHz	3.106 MHz	−0.0162 MHz

Error Sources? **Stark shift**

Rabi frequency v.s. Resonance frequency

Calibration of Lamb-Dicke Parameters

Simulation



Calculation

$$P(\Omega, \eta, \Delta, t) = \frac{\eta^2 \Omega^2}{\eta^2 \Omega^2 + \Delta^2/4} \sin^2 \left(\sqrt{\eta^2 \Omega^2 + \frac{\Delta^2}{4}} t \right)$$

Example: 3 ions with 3 phonons.

	$\eta_{j,k}$	Calibrated $ \eta_{j,k} $	Error
η_{11}	-0.0457	0.0457	0.00%
η_{12}	0.0776	0.0774	-0.26%
η_{13}	0.0625	0.0625	0.00%
η_{21}	0.0909	0.0908	-0.11%
η_{22}	-2.77×10^{-6}	0.0	-
η_{23}	0.0629	0.0629	0.00%
η_{31}	-0.0457	0.0457	0.00%
η_{32}	-0.0776	0.0774	-0.26%
η_{33}	0.0625	0.0625	0.00%

Calibration of Lamb-Dicke Parameters

Determine the sign of $\eta_{j,k}$

Coupling the ions with different phonon modes

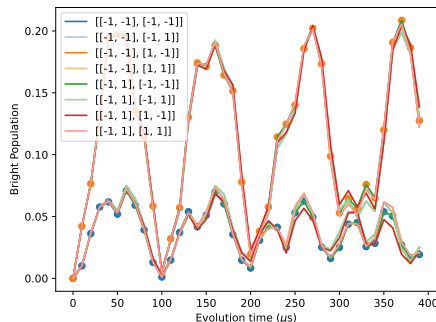
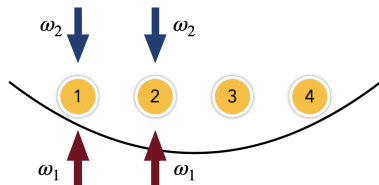
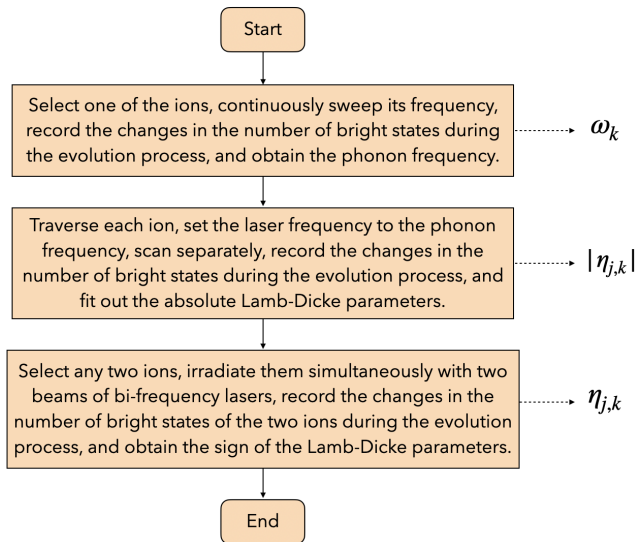


Figure: Example: 2 ions with 2 phonons

Complexity: 2^{N^2-1}



Segmented calibration → Complexity: $2N^2$

Summary



Thank you!



-  Bruzewicz, Colin D. et al. (June 2019). “Trapped-ion quantum computing: Progress and challenges”. en. In: *Applied Physics Reviews* 6.2, p. 021314. ISSN: 1931-9401. DOI: 10.1063/1.5088164.
-  Cirac, J. I. and P. Zoller (May 1995). “Quantum Computations with Cold Trapped Ions”. In: *Physical Review Letters* 74.20. Publisher: American Physical Society, pp. 4091–4094. DOI: 10.1103/PhysRevLett.74.4091.